

Spin and orbital angular momentum exchange in binary star systems

II. Ascending the giant branch: a new path to FK Comae stars

R. Keppens¹, S.K. Solanki², and C. Charbonnel³

¹ FOM-Institute for Plasma-Physics Rijnhuizen, P.O. Box 1207, 3430 BE Nieuwegein, The Netherlands (keppens@rijnh.nl)

² Max-Planck-Institut für Aeronomie, 37191 Katlenburg-Lindau, Germany

³ Laboratoire d'Astrophysique de Toulouse, 14 Av. E. Belin, 31400 Toulouse, France

Received 20 January 2000 / Accepted 28 April 2000

Abstract. Using the model by Keppens (1997), we investigate the angular momentum (AM) evolution in asymmetric binary star systems from Zero-Age Main Sequence times until at least one component has ascended the giant branch. We concentrate on stars ranging in mass from $0.9 M_{\odot} - 1.7 M_{\odot}$, in almost synchronous, short period systems ($P_{\text{orb}} < 9$ days). We address synchronization and circularization by tidal interaction, allowing for structural evolution and stellar winds. A Weber-Davis prescription is used to quantify the wind influence, thereby accounting for changes in its acceleration mechanism from the interplay of the evolving thermal-magneto-centrifugal effects. We identify a scenario for fast in-spiraling components with $d \ln P_{\text{orb}}/dt \simeq -\mathcal{O}(10^{-8})$ which is primarily driven by fast structural evolution as the heaviest component ascends the giant branch. This leads to the formation of contact systems, which ultimately coalesce and form FK Comae-like objects on relatively short timescales due to the continuing expansion of the primary.

The obtained mass loss rates and orbital period variations $d \ln P_{\text{orb}}/dt$ are confronted with their observed ranges. The predicted mass loss rates agree with the solar value on the main sequence and with the Reimers relation in the giant phase. Observations of period evolution in close, active binaries suggest, however, that other influences than those considered here must play an important role. Finally, we point out how the mass asymmetry of the binary system can be a crucial ingredient in the angular momentum evolution: while the primary dictates the spin-orbital AM exchange in the system, the slowly evolving lighter component can develop an efficient magneto-centrifugally driven wind and thereby drain the AM from the system.

Key words: stars: binaries: close – stars: evolution – stars: mass-loss – stars: rotation – stars: winds, outflows

1. Introduction

We continue the study of angular momentum (AM) exchange in binary star systems initiated by Keppens (1997, hereafter

Send offprint requests to: R. Keppens (keppens@rijnh.nl)

Paper I). Paper I introduced a straightforward extension of the MacGregor & Brenner (1991) model, used to study the AM evolution of *single* stars (Keppens et al. 1995), such that the AM balance in tidally coupled *binaries* could be investigated. With the structural evolution obtained from calculated evolutionary tracks as input, we use the model to quantify tidal interaction and wind driven angular momentum loss. Since Paper I concentrated on the model itself, along with illustrative calculations for two symmetric $1 M_{\odot} - 1 M_{\odot}$ systems from Pre-Main Sequence (PMS) times to the start of the ascent of the giant branch, we focus in this paper on asymmetric binaries from Zero-Age Main Sequence (ZAMS) times up to the giant phase.

As we intend to address issues related to synchronization, circularization, and wind effects, various earlier studies are of direct relevance in this context. Habets & Zwaan (1989) have investigated the puzzling question of asynchronous rotation in circularized binaries. One typically expects the components to synchronize before the orbit becomes circular. They identified periods of asynchronism in model calculations incorporating physical mechanisms much like the ones we account for. Schrijver & Zwaan (1991) used observations of close binary systems to compare the activity-rotation relation of single stars with otherwise identical component stars in binaries. They found evidence for enhanced magnetic activity. Since this is relevant for the stellar wind and the associated mass and angular momentum loss, it is our goal to quantify the wind effects accurately. Typically, a Skumanich relation (Skumanich 1972) or extrapolation thereof is used in quantifying the braking role of stellar winds. Since this relation does not allow for characterisations of the type of wind acceleration (thermal, magnetic, centrifugal), we adopt a Weber-Davis (Weber & Davis 1967) wind model. On top of quantifying the AM losses, this model predicts mass loss rates and wind types as the stellar structure adjusts to the prevailing circumstances. We will compare the predicted mass loss rates with the Reimers relation derived from observations of supergiants (cf. the review by Dupree & Reimers 1987) as well as with the known mass loss rate of our sun, of order $10^{-14} M_{\odot} \text{yr}^{-1}$. The obtained period changes will be confronted with those cataloged for chromospherically active binary stars (Strassmeier et al. 1993). The role of the stellar winds in late-type close binaries has also been stressed in studies by van 't Veer and Maceroni

(van 't Veer 1993; van 't Veer & Maceroni 1992; Maceroni 1993). It is well known how in synchronous systems, AM loss leads to counterintuitive spin up as the orbital AM is tapped most efficiently. Here we stress how, similarly, the changing structure can also become important for spin-orbital AM exchange.

The tidal coupling is ultimately responsible for synchronizing and circularizing the system. We actually consider almost synchronous systems in this paper. Paper I explained how our model could be used to evaluate different tidal theories against each other. Which kind of tidal interaction is at play in late-type main sequence stars is still a topic of active research: the equilibrium tide in stars with a convective envelope as studied by Zahn (1977; 1989) has been challenged by the hydrodynamical mechanism proposed by Tassoul & Tassoul (1992); and recently by Zahn's own dynamical tide as invoked for circularizing solar-type binaries (Goodman & Dickson 1998). A review of these three mechanisms is found in Tassoul & Tassoul (1996). Studies by Claret et al. (1995) and Claret & Cunha (1997) have compared their validity based on stellar data sets. Both Zahn's and Tassoul's formalism had several points of agreement with the observations. We defer from analysing the influence of the different mechanisms here and rather set forth to further elucidate the role of the different ingredients controlling the rotational evolution in binaries.

In Sect. 2, we repeat the model equations of Paper I to make this paper self-contained. A brief discussion of the most important parameters is given, along with all details on the wind calculation, in an appendix. The results are presented in Sect. 3, where three asymmetric systems are evolved from ZAMS to giant times. Sect. 4 confronts the period changes with observations and discusses the implications and shortcomings of the model from that viewpoint.

2. Model equations

For completeness, the full set of equations derived and presented by Keppens (1997) is repeated here. Each star ($i = 1, 2$ of mass M_i) can consist of an envelope and core region with respective angular momenta $J_{\text{env}}^{(i)} = I_{\text{env}}^{(i)}\Omega_{i,\text{env}}$ and $J_{\text{cor}}^{(i)} = I_{\text{cor}}^{(i)}\Omega_{i,\text{cor}}$. Here, I is the moment of inertia and the inherent assumption is that both regions rotate rigidly with angular velocity Ω . The orbital parameters are the eccentricity $0 \leq e \leq 1$, the semi-major axis a and orbital revolution rate $\Omega_{\text{orb}} = \sqrt{G(M_1 + M_2)/a^3}$, with associated orbital angular momentum $J_{\text{orb}} = \Omega_{\text{orb}}a^2\sqrt{1 - e^2}M_1M_2/(M_1 + M_2)$. G is the gravitational constant. The six quantities $[J_{\text{cor}}^{(1)}, J_{\text{env}}^{(1)}, J_{\text{cor}}^{(2)}, J_{\text{env}}^{(2)}, J_{\text{orb}}, e]$ are evolved according to

$$\begin{aligned} \frac{dJ_{\text{cor}}^{(i)}}{dt} &= -\frac{J_{\text{cor}}^{(i)}I_{\text{env}}^{(i)} - J_{\text{env}}^{(i)}I_{\text{cor}}^{(i)}}{(I_{\text{cor}}^{(i)} + I_{\text{env}}^{(i)})\tau_c^{(i)}} + \frac{2}{3}\Omega_{i,\text{env}}R_{i,\text{cor}}^2 \frac{dM_{i,\text{cor}}}{dt}, \\ \frac{dJ_{\text{env}}^{(i)}}{dt} &= +\frac{J_{\text{cor}}^{(i)}I_{\text{env}}^{(i)} - J_{\text{env}}^{(i)}I_{\text{cor}}^{(i)}}{(I_{\text{cor}}^{(i)} + I_{\text{env}}^{(i)})\tau_c^{(i)}} - \frac{2}{3}\Omega_{i,\text{env}}R_{i,\text{cor}}^2 \frac{dM_{i,\text{cor}}}{dt} \\ &\quad - \frac{J_{\text{env}}^{(i)}}{\tau_W^{(i)}} + S_{ij}, \end{aligned}$$

$$\begin{aligned} \frac{dJ_{\text{orb}}}{dt} &= -S_{12} - S_{21}, \\ -\frac{1}{e} \frac{de}{dt} &= \frac{15}{4}(1 + 2e^2) \frac{G}{\Omega_{\text{orb}}a^5} \\ &\quad \times \left[\frac{M_{1,\text{env}}R_1^2}{5} \frac{M_2R_1^3}{M_1a^3} \right. \\ &\quad \left. \sin \left(2 \frac{R_1^3}{GM_{1,\text{env}}\tau_{1,V}} [18\Omega_{\text{orb}}/11 - \Omega_{1,\text{env}}] \right) \right. \\ &\quad \left. + \frac{M_{2,\text{env}}R_2^2}{5} \frac{M_1R_2^3}{M_2a^3} \right. \\ &\quad \left. \sin \left(2 \frac{R_2^3}{GM_{2,\text{env}}\tau_{2,V}} [18\Omega_{\text{orb}}/11 - \Omega_{2,\text{env}}] \right) \right]. \quad (1) \end{aligned}$$

The torque exerted by star 2 on star 1 is modeled as

$$\begin{aligned} S_{12} &= \frac{3}{2} \frac{GM_1M_2}{M_1 + M_2} \frac{1}{a^3} \left(1 + \frac{3}{2}e^2 + \frac{15}{8}e^4 \right) \\ &\quad \times \frac{M_{1,\text{env}}R_1^2}{5} \frac{M_2R_1^3}{M_1a^3} \\ &\quad \sin \left(2 \frac{R_1^3}{GM_{1,\text{env}}\tau_{1,V}} [\Omega_{\text{orb}} - \Omega_{1,\text{env}}] \right), \quad (2) \end{aligned}$$

and similarly for S_{21} . For a discussion of the assumptions entering this formalism, we refer to Paper I. We repeat that the expression for the torque Eq. (2) and the corresponding evolutionary equation for the orbital eccentricity follows from an ad hoc description for the deformation of each component in the binary system. Tidal effects over one orbital revolution are modeled as deformations and misalignment angles that are constant over the orbit. This working hypothesis connects well to standard approaches for quantifying tidal effects, as explained in Paper I (Sect. 2.3). In particular, the equation for the eccentricity in Eqs. (1) captures in lowest order the essential dependence

$$-\frac{1}{e} \frac{de}{dt} \propto \frac{1}{\tau_V} \left(\frac{R}{a} \right)^8 \left[1 - \frac{11}{18} \frac{\Omega_{\text{env}}}{\Omega_{\text{orb}}} \right]. \quad (3)$$

This can be compared directly with fully self-consistent calculations as found e.g. in Eggleton et al. 1998, their Eq. (78).

The time integration requires as additional input an independent evolutionary calculation for each component, in the form of the evolving moments of inertia $I_{\text{env}}^{(i)}(t)$, $I_{\text{cor}}^{(i)}(t)$, stellar radius $R_i(t)$, core radius $R_{i,\text{cor}}(t)$ and mass $M_{i,\text{cor}}(t)$. $M_{i,\text{env}}(t)$ can then be expressed as $M_i - M_{i,\text{cor}}(t)$. Instantaneous values for the orbital parameters are obtained from the set (J_{orb}, e) . The evolutionary timescale of each component enters through the evolving stellar parameters, while an additional six timescales $\tau_c^{(i)}$, $\tau_W^{(i)}$, and $\tau_{i,V}$ appear explicitly in the set of Eqs. (1). In the following we provide a more detailed discussion of these time scales.

Firstly, the model equations allow for differentially rotating core and envelope regions, coupled through visco-magnetic mechanisms parametrized by their timescale τ_c (see Charbonneau & MacGregor 1992a, 1992b for a simulation of the physical processes involved). It was shown in Paper I that especially during Pre-Main Sequence phases, differential rotation

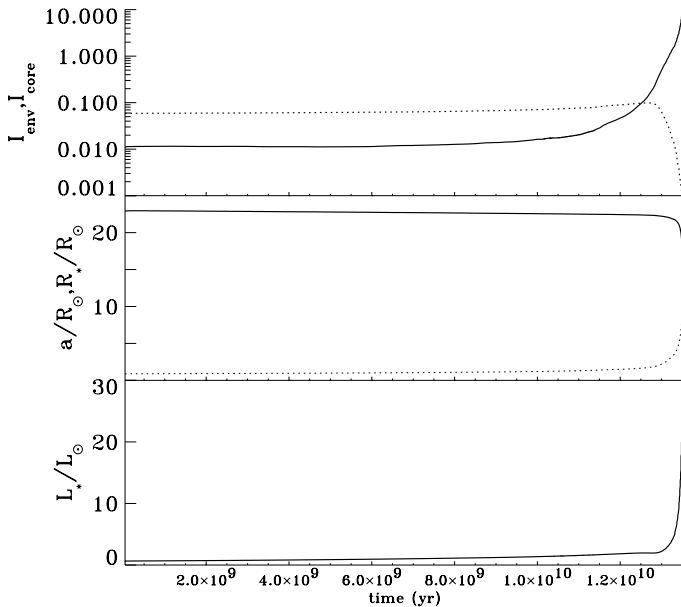


Fig. 1. Case I: two $1M_{\odot}$ stars. Plotted as a function of time are parameters of the structural evolution that serve as input, as well as the semi-major axis evolution: Top panel shows the moments of inertia of the stellar envelope I_{env} (solid) and core I_{cor} (dotted) in 10^{55} cgs units; Middle panel contains the input radius R_* (dotted) and the resulting values of the semi-major axis of the system a (solid); Bottom panel plots the stellar luminosity L_* .

can occur. It is influenced by τ_c and the buildup of a radiative core. Here, we concentrate on stages following the ZAMS where differential rotation is not too relevant and simply set $\tau_c^{(1)} = \tau_c^{(2)} = 10$ Myr, essentially yielding rigid rotation. This is further motivated by the more recent finding that AM studies for single stars using solid-body rotation throughout their PMS and Main Sequence (MS) evolution can account for the observed fast rotators around ZAMS times equally well as differential rotation (Bouvier et al. 1997). Also, mass transfer from envelope to core regions (or vice-versa) is insignificant on the MS and we in fact ignored the terms proportional to $dM_{i,\text{cor}}/dt$ for the calculations presented here.

Secondly, each component can be accompanied by a stellar wind characterized by its timescale $\tau_W^{(i)}(t)$. The wind exerts a braking torque on the stellar envelope region and is, in general, driven by a combination of thermal, magnetic, and centrifugal acceleration mechanisms. As it represents the only AM loss terms present in the system (1), we need a satisfactory quantitative prescription. We use an exact solution of the ideal magnetohydrodynamic equations from Weber & Davis (1967) to obtain instantaneous mass loss rates and wind braking torques. Since we make several observations related to the evolving stellar winds in what follows, we provide all further details about the wind solutions in the appendix. Note that we treat the wind of each star as if it were a single star of the relevant mass, radius and rotation rate, neglecting the enhanced magnetic activity in binaries proposed by Schrijver & Zwaan (1991).

Thirdly, a viscous timescale τ_V is used to parameterize the tidal interaction. It was pointed out in Paper I how different prescriptions for τ_V can recover the synchronization and circularization timescales known from standard tidal theories (Zahn 1977; Tassoul & Tassoul 1992). We will mostly deal with almost synchronous systems and use in practice $\tau_V = (MR^2/L)^{1/3}$, which is typical for the equilibrium tide raised on stars possessing convective envelopes. This means that the evolutionary calculation must also provide the changing luminosities $L_i(t)$.

For this paper, the evolutionary tracks were constructed with the Geneva-Toulouse evolutionary code which accounts for the following input physics. The initial helium content is determined by $Y=0.24+(\Delta Y/\Delta Z)Z$, with a value of 3 for the average relative ratio of helium to metal enrichment ($\Delta Y/\Delta Z$) during galactic evolution. The relative ratios for the heavy elements correspond to the mixture by Grevesse & Noels (1993) used in the opacity computations by Iglesias & Rogers (1996). Nuclear reaction rates are due to Caughlan & Fowler (1988). We use the OPAL radiative opacities from Iglesias & Rogers (1996), including the spin-orbit interactions in Fe and relative metal abundances based on Grevesse & Noels (1993). These tables are completed at temperatures below 10000 K with the atomic and molecular opacities by Alexander & Ferguson (1994). The mixing length parameter that enters the models is set to a value of 1.6. A grey atmosphere in the Eddington approximation is adopted as boundary condition. Below optical depth $\tau = 2/3$, full integration of the structure equations is performed.

3. Results

We simulate three different scenarios, in decreasing order of their initial orbital period $P_{\text{orb}} = 2\pi/\Omega_{\text{orb}}$. All systems start with a non-zero orbital eccentricity and an asymmetry between the rotation rates of the two stars. The last two cases, in addition, consider mass-asymmetric binaries.

3.1. Pseudo-synchronized $1 M_{\odot} - 1 M_{\odot}$ system

Case I starts from two ZAMS solar mass stars with orbital period $P_{\text{orb}} = 9$ days and $e = 0.05$. The symmetry is deliberately broken by setting the equatorial rotational velocities equal to 30 km s^{-1} and 1 km s^{-1} , which is roughly 15 times and half the present solar rotation rate, respectively. One component thereby rotates faster than the orbital rotation rate, the other slower. The system of Eqs. (1) is then integrated using the evolving moments of inertia I_{env} and I_{cor} , radius R_* , and luminosity L_* (used in the tidal timescale only) as shown in Fig. 1. As is well-known, the giant branch ascension is marked by rapid structural evolution, where the moment of inertia of the expanding envelope becomes much larger than I_{cor} . Due to the collapsing core, the situation quickly reverses from the prevailing conditions during the MS, where I_{cor} dominated I_{env} . The time integration is halted when the size of at least one star, and in this case both component stars, becomes comparable to the semi-major axis. We then typically have an order of magnitude increase in

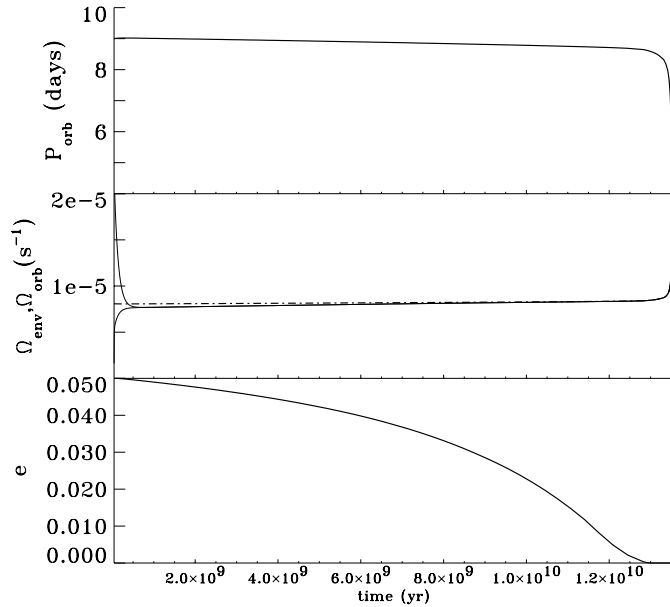


Fig. 2. Case I: the calculated evolution of (top) orbital period, (middle) the revolution rates (each component as a solid line; orbital Ω_{orb} dash-dotted) and (bottom) the eccentricity.

stellar radius and luminosity from the ZAMS to the end of the integration.

The resulting AM evolution of the binary system is seen in Fig. 1, where the semi-major axis a is plotted, and in Fig. 2 where essentially the same information is shown in terms of P_{orb} , Ω_{orb} , along with the eccentricity $e(t)$. The middle panel of Fig. 2 clearly shows how both component stars are rapidly forced to (pseudo-) synchronization: they all end up rotating close to, but slightly slower, than the orbital revolution rate. In effect, the initial asymmetry of the system disappears and we end with symmetric solar mass binaries as presented in Paper I. As pointed out there, a small degree of asynchronism is maintained during most of the MS evolution. Also, during the MS evolution the wind driven angular momentum loss is still very solar-like (mostly thermally driven wind, with magneto-centrifugal effects that are only a factor of $\simeq 2.5$ stronger than solar) – hence weak. As a result, a rather modest period decrease with $d \ln P_{\text{orb}}/dt \simeq -2.5 \times 10^{-12} \text{yr}^{-1}$ takes place. Note that unlike the spin down expected for a star in isolation when AM is lost due to its wind, the almost synchronous binary system ends up rotating faster when winds are present. AM is preferentially taken out of the orbit instead, while the component stars are forced to spin up due to the synchronization. Note also that during the entire stay of the stars on the MS, circularization is not achieved.

The evolution of the orbit changes drastically when both components ascend the giant branch. $d \ln P_{\text{orb}}/dt$ then increases and reaches values up to $\simeq -2.6 \times 10^{-8} \text{yr}^{-1}$, so that the two stars approach each other rapidly, accompanied by strict synchronization and circularization. The strong tidal coupling keeps the system synchronous: although the torque terms given in Eq. (2) vanish for *exact* synchronisation, the slightest dif-

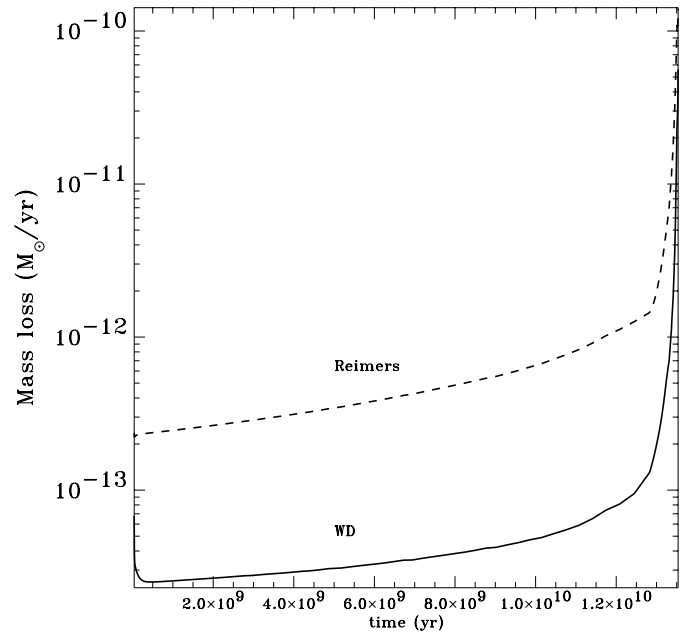


Fig. 3. Case I: the mass loss rate of each component in solar masses per year as predicted by the Weber-Davis wind model (solid) and by the Reimers relation (dashed). Approximate agreement is reached in the giant phase, where the Reimers relation is expected to represent stellar mass loss rates most accurately.

ference between the orbital Ω_{orb} and envelope revolution rate $\Omega_{i,\text{env}}$ is sufficient to drive them back to isorotation.

The fast expansion of both envelope regions again acts oppositely to what is expected for stars in isolation¹: while a single star would react by rotating slower, the synchronized system in fact redistributes spin with orbital angular momentum very effectively, thereby conserving the total AM (except for some modest wind AM loss). Both stars spin up quickly and their winds acquire a strong centrifugal component. This also accelerates the approach, but turns out to be of marginal interest for the case shown here. The rapid approach is very suggestive of the formation of contact systems. We note that Stępień (1995) stressed the wind associated AM loss to form contact systems from synchronized, detached binaries. In that study, the loss formula was calibrated using spin down rates of single stars. In contrast, we find scenarios for which the wind has little effect on the approach of the two stars, while their structural evolution plays the dominant role.

This conclusion depends on whether the wind associated mass loss predicted by the model is adequate. This can be deduced from Fig. 3. As expected, it is close to solar values during much of the MS, namely $\mathcal{O}(10^{-14}) M_{\odot} \text{yr}^{-1}$, but reaches $\dot{M} \simeq 5 \times 10^{-11} M_{\odot} \text{yr}^{-1}$ at the end. For comparison, the

¹ We hereby correct an interpretation error present in Paper I, where the initial ascent on the giant branch led to similar effects. Keppens (1997) wrongly suggested that this was due to core collapse, but the vanishing I_{cor} rules out that interpretation.

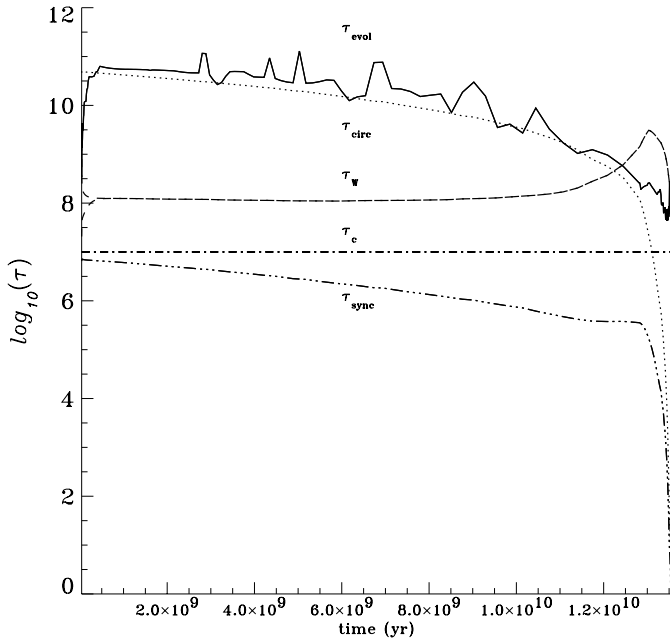


Fig. 4. Case I: the various timescales that influence the AM balance within the binary on a logarithmic scale, with τ in years. Plotted are the evolution timescale τ_{evol} (solid), circularization timescale τ_{circ} (dotted), wind timescale τ_W (dashed), coupling timescale τ_c (dash-dotted), and synchronization timescale τ_{sync} (— · — · —).

Reimers relation deduced observationally for red supergiants ($M_* > 4M_\odot$ and $R_* > 40R_\odot$) in binary systems,

$$\dot{M} = 4 \times 10^{-13} \frac{(L_*/L_\odot)(R_*/R_\odot)}{M_*/M_\odot} [M_\odot \text{yr}^{-1}], \quad (4)$$

is plotted as a dashed line in Fig. 3. At the later giant phases, which is where the Reimers relation is expected to be a good indication of the actual mass-loss rate, we reach a satisfactory quantitative agreement (i.e., the difference between the two mass-loss rates is only a factor of 2.5 at the end of the calculation). Note that the time-integrated mass loss is still negligible relative to the ZAMS mass, so we did not require the stellar mass M_* to change in the course of the evolution.

Finally, Fig. 4 plots the evolving timescales that are present in the system of equations: the coupling timescale τ_c (kept fixed), the wind timescale τ_W , and the evolutionary timescale derived as

$$\tau_{\text{evol}} \equiv \min \left[(d \ln R_*/dt)^{-1}, (d \ln I_{\text{env}}/dt)^{-1}, (d \ln I_{\text{cor}}/dt)^{-1} \right]. \quad (5)$$

The irregularities in τ_{evol} in Fig. 4 reflect minor remaining inaccuracies in the evolutionary tracks at our disposal. However, as can be seen in Fig. 1, the tracks are sufficiently smooth for doing meaningful calculations. τ_{evol} , being a differential quantity, blows up such irregularities disproportionately.

The plotted circularization time is (see Paper I)

$$\tau_{\text{circ}} \equiv \frac{11}{42} \left[\tau_{1,V} \left(\frac{a}{R_1} \right)^8 + \tau_{2,V} \left(\frac{a}{R_2} \right)^8 \right], \quad (6)$$

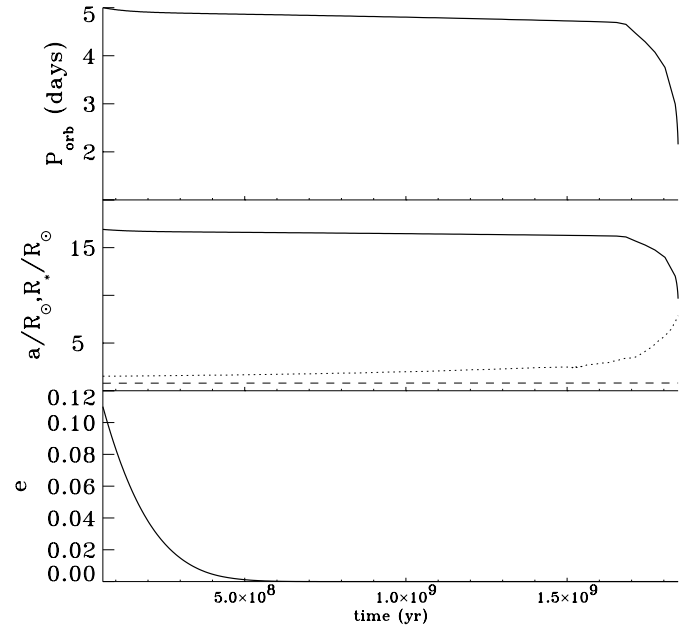


Fig. 5. Case II: a $1.7 M_\odot - 0.9 M_\odot$ system. As in Fig. 2, orbital period (top) and eccentricity (bottom) are plotted; with the semi-major axis a (solid) and input radii $R_{1.7M_\odot}$ (dotted) and $R_{0.9M_\odot}$ (dashed) being displayed in the middle panel.

while the synchronization timescale is taken to be

$$\tau_{1,\text{sync}} \equiv \frac{5}{3} \frac{I_{1,\text{env}}}{M_1 R_1^2} \frac{M_1}{M_2} \frac{M_1 + M_2}{M_2} \left(\frac{a}{R_1} \right)^6 \tau_{1,V}. \quad (7)$$

The evolution of these timescales supports the AM evolution scenario as outlined above: the system is essentially synchronized, with only modest wind driven AM loss during the MS. At the giant branch ascension, the lowest energy state of a circular orbit with synchronous rotation is enforced, with the evolutionary timescale dominating the process as $\tau_{\text{evol}} < \tau_W$. Only at the very end of our integration do the two time scales become comparable again. Therefore, during the period of rapid structural evolution, the wind AM loss remains fairly low, even though the associated mass loss continues to increase quickly (cfr. Fig. 3). This is possible due to the different dependencies of the mass loss rate and the wind time scale on particularly the stellar radius (see appendix).

3.2. Synchronized $1.7 M_\odot - 0.9 M_\odot$ system

Case II introduces a mass asymmetry and places the components such that the orbital period is equal to 5 days, with an eccentricity of 0.11. Although we start in a state of non-synchronous rotation, with equatorial velocities set to 10 and 14 km s^{-1} , the very effective tidal torques and associated short synchronization timescales lead to almost immediate synchronization. Note in Fig. 5 how circularization now occurs within several 10^8 yrs, while both stars are still on their MS. The faster rotation (about 5 times solar) also involves a more effective wind-driven AM loss, but it still leads to only $d \ln P_{\text{orb}}/dt \simeq -3.3 \times 10^{-11} \text{ yr}^{-1}$ before the heavy component ascends the giant branch. Essen-

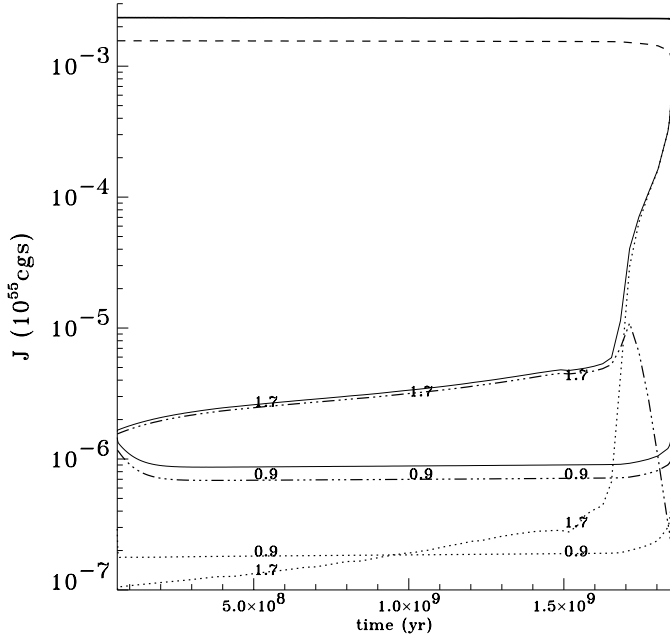


Fig. 6. Case II: The entire AM balance as a function of time – note the logarithmic scale. The thick solid line at the top is the total AM J_{TOT} , with the orbital AM J_{orb} multiplied by $2/3$ as a dashed line underneath. The thin solid lines at bottom are the total spin AM in each component star, with their individual contributions from envelope and core regions as dotted and $-\cdot-\cdot-$ lines, respectively.

tially the same observations as in Case I hold when this primary expands suddenly: the stars approach each other at a rapidly increasing rate that reaches $d \ln P_{\text{orb}}/dt \simeq -5 \times 10^{-8} \text{yr}^{-1}$. Now, the lighter secondary is simply enforced to corotate at the same rotation rate, with spin-orbital AM exchange induced by the primary. The entire angular momentum balance is shown in Fig. 6 (note the logarithmic scale). The total AM can decrease only due to the stellar winds. As Fig. 6 shows it decreases only slightly (2% decrease between the beginning and the end of our integration). Except at the very end, almost all the AM resides in the orbit. Note that the orbital AM curve has been multiplied by $2/3$ in Fig. 6 to help distinguish it from the total AM. In the giant evolutionary stage of the $1.7 M_{\odot}$ star, a non-negligible fraction of the total AM resides in that star’s envelope – the core collapses and no longer plays a significant role in the AM balance. In response to the growing $J_{\text{env}}^{(1)}$, spin AM is exchanged with the orbit: the increase in $J_{\text{env}}^{(1)}$ is balanced with a J_{orb} decrease, keeping the total AM equal. The J_{orb} decrease lowers a , and due to the synchronization, both stars are forced to spin up. This again favours spin-orbital AM exchange, as the faster rotation also increases $J_{\text{env}}^{(1)}$.

The wind character of the stars is such that most AM is lost from the primary, with an important centrifugal component in its driving mechanism, especially at the giant stage spin up. The secondary has a modest magneto-centrifugal wind which simply results from the enforced corotation at about 5 times the solar rate. Mass loss rates for the $0.9 M_{\odot}$ star stay at $\mathcal{O}(10^{-14})$ solar masses per year throughout, while the heavier star begins

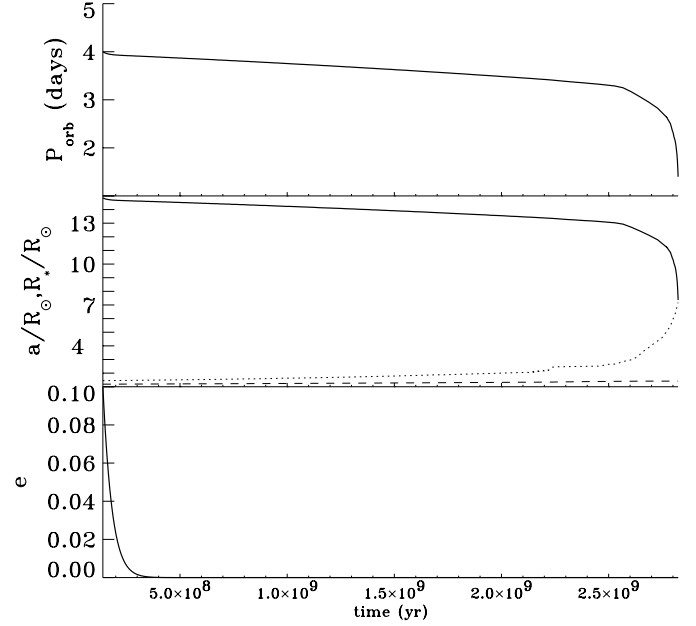


Fig. 7. Case III: a $1.5 M_{\odot} - 1.25 M_{\odot}$ system. Note the rapid circularization (as in Fig. 5) and noticeable orbital period change already on the main sequence.

at 10^{-13} with an increase up to 3×10^{-11} . Overall, the evolution is not unexpectedly different from the previous case, with the primary dominating the evolution.

Note that the evolutionary tracks for the $1.7 M_{\odot}$ primary indicate that such stars have an extremely shallow outer convection zone during their MS phase. This might hamper dynamo action and thus stifle the wind. Since during the MS evolution, the influence of the wind is minute (see Fig. 6), we do not expect that this alters our results.

3.3. Synchronized $1.5 M_{\odot} - 1.25 M_{\odot}$ system

Case III considers two stars with masses $> 1 M_{\odot}$ in a $P_{\text{orb}} = 4$ days, eccentricity $e = 0.1$, binary configuration. Initial equatorial velocities were taken to be 30 and 14 km s^{-1} , but as in Case II, this difference in rotation rate disappears almost instantly. Hence, the binary system of interest is one of almost rigidly rotating (due to the short τ_c), essentially synchronized $1.5 M_{\odot} - 1.25 M_{\odot}$ stars.

The evolution is summarized in Fig. 7. Note the fast circularization: taken together with the results shown in Paper I – where the PMS evolution of both a 15 day and a 5 day period system with two solar-mass stars did not show strong circularization – we may conclude that non-zero eccentricities for systems with $P_{\text{orb}} \lesssim 5$ days can only occur before or close to ZAMS times. Systems with larger mass obviously circularize more rapidly for a given period, which follows from the factors $(a/R)^8$ in the expression for the circularization time scale (Eq. (6)).

It is also clear from Fig. 7 that before the heaviest component enters the giant phase, a noticeable influence of the stellar wind AM loss is already present (compare with Figs. 2, 5). We

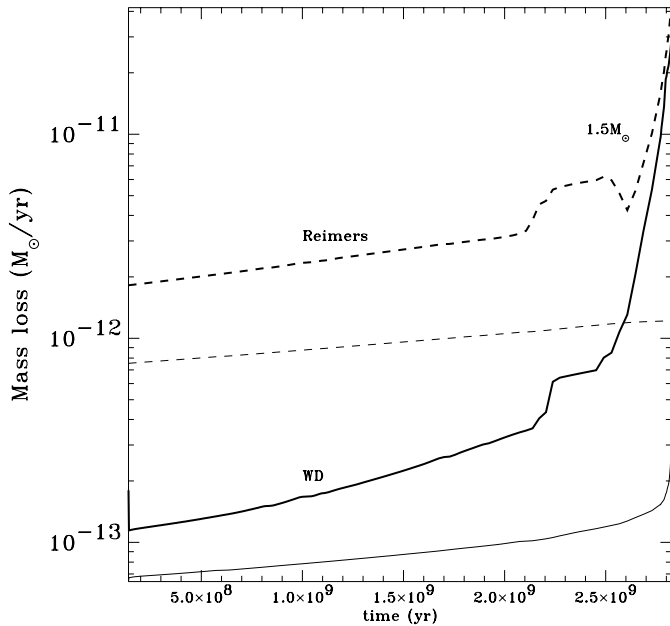


Fig. 8. Case III: mass loss rates for both component stars (solid), with the Reimers relation as dashed lines for comparison. Only the evolved primary (thick curves) has significant mass loss associated with its wind.

now observe a $d \ln P_{\text{orb}}/dt \simeq -6.8 \times 10^{-11} \text{yr}^{-1}$ on the MS. It turns out that the wind of the lighter secondary star is the main loss term responsible for this MS period decrease (or spin up). Its wind character is magneto-centrifugal, while the primary star has a much weaker mainly thermal-centrifugal wind. In the appendix, we show the loss terms associated with both winds as a function of time in Fig. 11, as well as the evolving wind character in Fig. 12. It should be noted that because these stars are synchronously rotating, the difference in wind character ultimately relates to their different radii and internal structure. The appendix lists in detail how these quantities can alter the wind properties. The associated mass loss is plotted in Fig. 8, again in comparison with the Reimers relation (Eq. (4)). Interestingly, the secondary has a far smaller mass loss rate in spite of dominating the angular momentum loss for most of the evolution. Only after the primary leaves the MS does its wind provide the dominant AM loss. As in Fig. 3, the lighter component has more MS solar-like mass loss with an increase at the end when stronger centrifugal forces are at play. Not unexpectedly, the agreement between the Weber-Davis and the Reimers prescription is again only reached in the giant phase (for the primary). The bumps between 2.1 and 2.6×10^9 years in the mass loss rate are related to the characteristic changes in luminosity $L_{1.5M_{\odot}}(t)$ and radius $R_{1.5M_{\odot}}(t)$ that signal the end of the MS phase.

The evolution of the various timescales is plotted in Fig. 9. The ordering of the wind timescales (the shorter being the one of the secondary) confirms the observation from above: the lighter component plays a crucial role in the AM balance of the system. Similar to Cases I and II, when the heavy component starts its phase of rapid evolution, effective spin-orbital

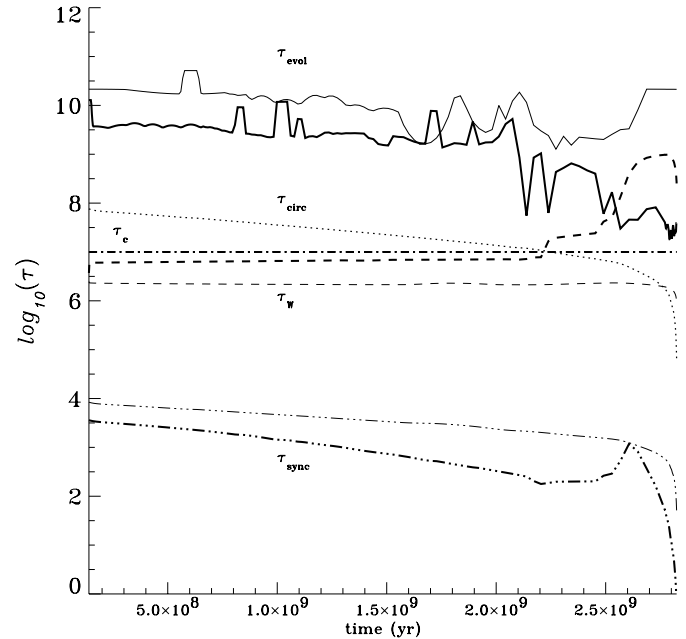


Fig. 9. Case III: the various timescales (as in Fig. 4), with τ_{evol} , τ_W , and τ_{sync} plotted for each component star. The thicker lines are for the primary.

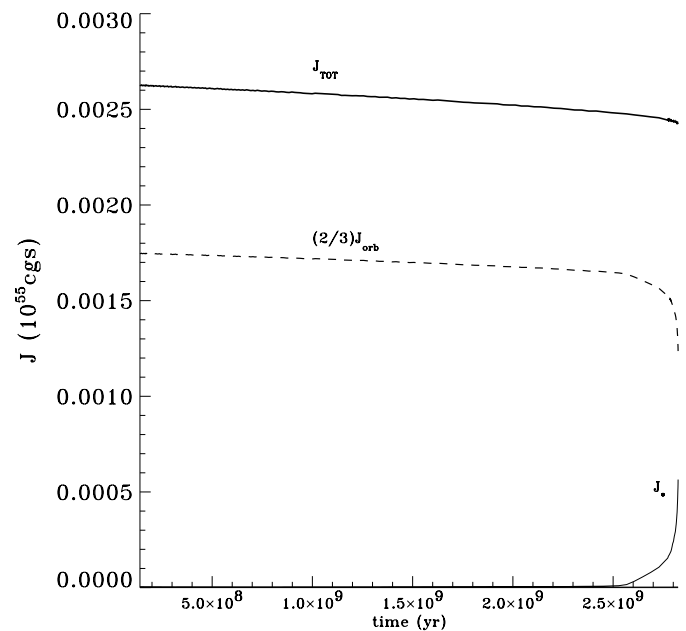


Fig. 10. Case III: the AM balance plotted as the total AM J_{TOT} , orbital AM J_{orb} (multiplied by 2/3 for easier visibility), and the spin AM of each component. In this linear scale, only the spin AM of the $1.5 M_{\odot}$ primary component shows up as it induces strong spin-orbital AM exchange when entering the giant phase.

AM exchange sets in and a period decrease of $d \ln P_{\text{orb}}/dt \simeq -7.3 \times 10^{-8} \text{yr}^{-1}$ is reached. The spin-orbital AM exchange can best be seen in Fig. 10, where we plot the total AM, the orbital AM, as well as the AM of each component. While the secondary does not show up in the scale used in that figure, the

giant-branch ascension of the primary clearly dictates the process. Of course, the overall decrease of the total AM balances the loss terms shown in Fig. 11.

4. Discussion and conclusions

We have considered the AM evolution of late-type binaries on the MS and while ascending the giant branch. Whereas the usually small changes in orbital parameters on the MS are caused by AM loss through the wind(s) of the stars and spin-orbit coupling, on the giant branch the much larger changes of the semi-major axis are due to the expansion of the stellar envelope(s) and spin-orbit coupling.

Our investigation allows us to test the Weber-Davis description in a rather different parameter regime than the solar case for which it was originally proposed, namely for giants. A comparison with the Reimers formula, derived from supergiant winds, shows increasingly good correspondence between the two descriptions as the star moves up the giant branch. This confirms that the basic assumptions underlying our wind model (Weber-Davis wind with the assumption of a constant coronal temperature) are acceptable over a large part of the Hertzsprung-Russell diagram.

Our calculations reveal that the orbital decay is particularly rapid when one of the components leaves the MS and expands. This quickly leads to the formation of contact systems driven by spin-orbit coupling while one progenitor star ascends its giant branch. The further merging process could produce a single, evolved, rapidly rotating giant object like an FK Comae type star. It is of interest to contrast this scenario with the one proposed by Stępień (1995). He suggested that contact systems form while both components are in their MS stage – necessarily through wind-driven AM loss – and that this formation scenario typically takes several Gyr. In contrast we expect this formation phase to last for only a short time before the components coalesce and form FK Comae type stars, since in our scenario the primary is already ascending its giant branch.

According to the same author, the contact phase itself must also be of the order of a few Gyr. For more massive stars, this is shorter than their MS lifetime, so that the stars merge and become an FK Comae object only after one of them reaches the giant phase. Our calculations suggest that this contact phase lasts for only a short time before the components coalesce and form FK Comae type stars. Also, the initial orbital period of the system can be considerably longer according to our scenario than according to that of Stępień: even the 9 day period system of two solar mass stars (Case I) becomes a contact system eventually. Note that the masses of the component stars do not influence the fate of the system. In all cases studied here, the MS wind is not a factor in the contact system formation. The evolution of the stellar structure is thus an important ingredient for calculations of the orbital evolution of binaries. However, as we shall see below, the ingredients of our model are still not sufficient to reproduce the short-term orbital-period changes observed in some systems. Moreover, our calculations apply to systems where the total mass lost during the primary MS phase

is negligible. Observations reveal that this is not true in general, and the relative importance of mass loss versus angular momentum loss may be a decisive factor in the ultimate fate of the system. While all cases considered have a contact system as their likely outcome, an evolving mass ratio may instead lead to conventional slow-timescale Roche lobe overflow without a final merger.

All three considered cases have components not too different in mass from the sun, with periods ranging from 9 down to 1 day during the simulated timeframe. While we concentrated here on systems starting from ZAMS times until one component becomes a giant star, we include the two cases reported in Paper I in the discussion. There, we evolved two symmetric $1 M_{\odot} - 1 M_{\odot}$ systems all the way from PMS times to the beginning of their ascent of the giant branch. These systems started with a 15 day and a 5 day period, respectively, with an initial eccentricity of $e = 0.05$.

As we account for stellar winds emanating from hot coronae, one observational motivation for studying these systems arises from the many chromospherically active binary star systems. Strassmeier et al. (1993) conveniently cataloged those systems with at least one late-type component with Ca II H and K emission in its spectrum. We comment on a few of these systems with listed $d \ln P/dt$ values (from Hall et al. 1980) and copied their parameters from the catalog into Table 1. Most systems in this table were originally studied by Popper (1988, 1990). Note that $d \ln P/dt$ can have either sign.

For those systems with periods around 7–9 days, Case I studied in this paper may be relevant. The three tabulated systems are roughly synchronised, with MM Her having $\Omega_* \geq \Omega_{\text{orb}}$. In our model calculations, the only time where this ordering of rotation rates occurred is on the PMS and for a limited time around ZAMS. A faster rotation at ZAMS times was also advocated by Habets & Zwaan (1989). Further, we found that in this range of orbital periods, non-zero eccentricities remain possible on the MS, so that the eccentricity of MM Her is not entirely in contradiction with our theory. Zahn & Bouchet (1989) concluded that orbit circularization takes place during contraction in the Hayashi phase. As indicated in Paper I, the two PMS evolution scenarios studied did not include that phase and started when the first radiative core region had developed. More definite statements about circularization can be made using our model when we have full evolutionary tracks extending from Hayashi contraction all the way to giant expansion.

The values of the period changes are an order of magnitude larger than the largest changes obtained in the model. SS Boo even has a positive $d \ln P/dt$ value, which in our model is only observed during the PMS phases as shown in Paper I. In a 5-day period, mass-symmetric system, we there got $d \ln P/dt \simeq +6.8 \times 10^{-10} \text{yr}^{-1}$. That period change was essentially due to the contraction of the component stars, leading to the (again counterintuitive) spin down of the close binary system due to spin-orbital exchange. Both component stars did spin up during those times, as the coupling was not sufficient to enforce corotation. A similar spin down effect in synchronous systems could arise from mass accretion (ignored in our model).

Table 1. A selection of chromospherically active binaries from Strassmeier et al. (1993), with reported period changes. The systems are ordered with decreasing orbital period (listed in days).

Name	Spectral type	Masses (M_{\odot})	Radii (R_{\odot})	P_{phot}	P_{orb}	e	$d \ln P/dt$ (yr^{-1})
AW Her	G2/G8IV	1.25/1.33	2.4/3.2	–	8.8	–	-0.7×10^{-6}
MM Her	G2/K0IV	1.22/1.28	1.6/2.8	7.936	7.96	0.04	-1.4×10^{-7}
SS Boo	G0V/K0IV	0.97/0.97	1.3/3.3	sync	7.6	0.0	$+2.16 \times 10^{-7}$
Z Her	FV/K0IV	1.61/1.31	1.85/2.73	3.96	3.99	0.0	-2.84×10^{-8}
UX Com	G2/K1IV	1.02/1.2	1/2.5	sync	3.6	0.0	-2×10^{-6}
GK Hya	F8/G8IV	1.25/1.34	1.5/3.4	sync	3.6	0.0	-2.28×10^{-7}
TY Pix	G5IV/G5IV	1.22/1.2	1.6/1.7	3.32	3.2	0.0	$+1.7 \times 10^{-7}$
PW Her	F8-G2/K0IV	1.17/1.5	1.4/3.8	sync	2.88	0.0	-4.9×10^{-7}
RT And	F8V/K0V	1.5/0.99	1.17/0.84	sync	0.63	0.09	-1.17×10^{-7}

The difference in magnitude of the observed and theoretical period changes and the fact that dP/dt can have either sign rather supports an interpretation of these period changes in terms of stellar magnetic activity (Hall 1991, Applegate 1992, Lanza et al. 1998).

For the shorter period systems (around 3–4 days), our Cases II and III may be of interest. Again we do not attain the high $d \ln P/dt$ values, we find typically $d \ln P/dt \simeq -\mathcal{O}(10^{-8})$, and could make similar remarks as above about both occurring signs. These systems are circularized, as expected from the model. Z Her has a $d \ln P/dt$ value that is in accord with the maximal value predicted by our model. However, this system has the peculiarity that the more evolved, cooler K star is the less massive one. Presumably, Z Her started off as a normal binary with the K star being more massive, so that significant mass loss must have taken place to reverse this situation. This scenario is not present in the Case studies, where always the total amount of mass lost from the system during the simulated time period was negligible. Z Her therefore serves to show that this is not generally applicable and the mass loss rate may be the more dominant effect in the binary evolution. In TY Pix, the stellar rotation rate is slightly lower than the orbital rotation rate, something we could tentatively relate to the small asynchronism witnessed in Case I. Finally, the shortest period system listed in Table 1 presents us with a new puzzle: it lists a non-zero eccentricity.

In summary, the observations indicate several areas where our case-studies need extra physical input. In order to explain the observed period changes on the MS fully within the context of our model, more effective wind-driven AM loss is needed. In that respect, the Strassmeier catalog mentions a derived dipole field for UX Com of 579 G, and for RT And of 526 G, both at least an order of magnitude higher than the highest value used in our wind models. In addition, Schrijver & Zwaan (1991) determined observationally that the magnetic activity of stars in tidally interacting binaries is enhanced with respect to similarly rotating stars in isolation. This suggests that we need to allow for a more complicated ‘dynamo relation’ (as used in the Weber-Davis models) where the properties of the secondary enter in some way (this applies equally to the angular momentum loss rates derived empirically from single stars, used by e.g., Stępień 1995, van ’t Veer & Maceroni 1988). The resulting stronger AM loss, in addition to the structurally dominated spin-orbital ex-

change seen in the cases studied, could indeed bring the negative $d \ln P/dt$ values in order of magnitude agreement. On the other hand, the detailed magnetic topology in close binary systems may include the formation of large ‘dead’ zones. Just as in single star studies (Solanki et al. 1997), no mass and AM is lost from these zones, so that the loss rates do not necessarily increase with field strength (Moss 1986). The alternative to making the wind-driven loss more effective, is to invoke a mechanism such as that proposed by Applegate (1992): binary period changes resulting from the orbital response to variations in the shape of a magnetically active component. However, significant shape deformations would again require kG magnetic fields.

Therefore, our conclusions are as follows. First, our model can successfully be used for investigating the AM evolution in both symmetric and asymmetric binaries. During periods of rapid structural evolution (PMS contraction and giant ascension) we find modest to strong spin-orbital AM exchange. The influence of stellar winds, as they evolve in character due to changes in the thermal-magneto-centrifugal driving, can be quantified with mass loss rates and period variations. The obtained mass loss rates agree with the solar value on the MS and with the Reimers relation in the giant phase. Our calculations indicate a viable path to the formation of contact systems. These are expected to coalesce and form FK Comae-like objects on relatively short timescales due to the continuing expansion of the primary. According to this path binaries with considerably larger initial periods can end up as FK Comae stars as compared to the scenario proposed by Stępień (1995). We identified a case where the mass asymmetry was of interest to the global AM evolution: Case III had its primary dictating the spin-orbital AM exchange, while the secondary shed the AM from the system in the form of a magneto-centrifugal wind. Our model results, confronted with the observational evidence on chromospherically active binaries, suggests that possibly stronger winds or other mechanisms for changing the orbital AM, at least on short time scales, are at play in these systems.

Meaningful modifications and extensions of our model could investigate AM scenarios in other than solar-type star binary systems, where a wealth of observations exists on mass loss rates (see the review by Cassinelli & Lamers 1987) and where other types of wind (radiation driven) are at play.

Acknowledgements. Computer time on the Cray C90 was sponsored by the Dutch ‘Stichting Nationale Computerfaciliteiten’.

Appendix: Weber-Davis wind model

The Weber-Davis model (Weber & Davis 1967) is an ideal magnetohydrodynamic (MHD) solution for a thermal-magneto-centrifugally driven stellar wind from a star with radius R_* and mass M_* , which rotates with angular velocity Ω_* . In particular, this model solves for the steady-state ($\partial/\partial t = 0$) expansion of the magnetized stellar corona using an axisymmetric ($\partial/\partial\phi = 0$) and polytropic description in the equatorial plane. Hence, $p/p_o = (\rho/\rho_o)^\alpha$, where p is the pressure, ρ is the density, and α is the polytropic index, while $\partial/\partial\theta = 0$, and $v_\theta = 0$, with θ the spherical polar angle.

As pointed out in Belcher & MacGregor (1976), a Weber-Davis wind is completely determined by the set of six dimensionless unknowns $x_1, x_2, x_3, x_4, x_5, x_6$ defined as

$$[v_{r_o}/a_o, v_{\phi_o}/a_o, r_s/r_o, v_{r_s}/a_o, r_f/r_o, v_{r_f}/a_o],$$

for given values of the five parameters c_1, c_2, c_3, c_4, c_5 , namely

$$\left[\alpha, a_o, \Omega_* r_o/a_o, \sqrt{2GM_*/r_o}/a_o, \left(B_{r_o,*}/\sqrt{4\pi\rho_o} \right)/a_o \right].$$

In these formulae, the subscript o refers to (values at) the reference radius taken at $r_o \equiv 1.25R_*$. With a_o the base sound speed, the last three parameters are dimensionless ratios of the rotational speed at the reference radius, the escape speed at r_o , and the base radial Alfvén speed to the local sound speed. The six unknowns are the dimensionless base radial and azimuthal velocity, plus the location of and the radial expansion velocities at the two critical points $[r_s, r_f]$. At these *slow* and *fast* critical radii, the radial speed goes transonic, in the MHD sense.

We explained earlier (Keppens et al. 1994; 1995) that we constructed a table of Weber-Davis wind solutions starting from a reference solar wind solution with $\alpha = 1.13$, $a_{o,\odot} = 167 \text{ km s}^{-1}$, based on a number density of 10^8 cm^{-3} and coronal temperature $1.5 \times 10^6 \text{ K}$ at $r_{o,\odot} = 1.25R_\odot$, for a rotation rate of $\Omega_\odot \simeq 3 \times 10^{-6} \text{ s}^{-1}$ and coronal field strength $B_{r_{o,\odot}} \simeq 2 \text{ G}$.

The table of solutions is a two-dimensional grid extending the range of the centrifugal c_3 and magnetic c_5 parameters from 0.5 to 60 times their solar values. The instantaneous values of the mass loss rate and the wind timescale τ_W for a stellar wind are obtained as follows. The current rotation rate and stellar radius yield a centrifugal parameter

$$c_3 = f_3 \times c_{3,\odot} = (\Omega_*/\Omega_\odot)(R_*/R_\odot)c_{3,\odot}.$$

Similarly, we assume a saturated dynamo relation so that $B_{r_o,*}(\Omega_*)$ increases linearly with Ω_* for $\Omega_* < 20\Omega_\odot$, but saturates at a constant value for more rapid rotation. When we additionally incorporate flux conservation, we write for the magnetic parameter

$$c_5 = f_5 \times c_{5,\odot} = \min[(\Omega_*/\Omega_\odot), 20] f_B(R_*^2(t_{\text{ref}})/R_*^2)c_{5,\odot}.$$

It should be noted that the three cases presented here never had $\Omega_* > 20\Omega_\odot$, so that in practice the dynamo relation is

linear. In this latter equation, the reference time t_{ref} for the flux conservation is taken as the solar age $t_\odot = 4.5 \times 10^9 \text{ yr}$ if available from the evolutionary tracks, and equal to the stellar ZAMS time of minimal radius otherwise. The factor f_B is a pure multiplicative factor to allow for a higher or lower coronal field strength than the adopted solar values, but is always taken $f_B = 1$ in the calculations presented here. Under the assumption that all other quantities (α, a_o or base temperature and density, and c_4 or base escape speed) are given by their solar analogues, we then obtain the mass loss rate as

$$\dot{M} = 4\pi\rho_{o,\odot}a_{o,\odot}r_o^2x_1,$$

and the timescale for the wind spin down of the stellar envelope region with moment of inertia I_{env} as

$$\tau_W = \frac{I_{\text{env}}c_3}{\frac{8\pi}{3}\rho_{o,\odot}a_{o,\odot}r_o^4x_1 \left[x_2 - \frac{c_2^2}{x_1^2}(x_2 - c_3) \right]}.$$

When deriving these equations, we used several properties of the Weber-Davis wind model, like the constancy of the mass flux, and other known constants of motion. For the standard solar values, the mass loss rate turns out to be $2.94 \times 10^{-14} M_\odot \text{ yr}^{-1}$.

What is immediately evident from these formulae and the way we use the grid of Weber-Davis wind models to obtain mass loss rates and wind braking torques is that we *neglect the obviously important changes in coronal temperature, density, and escape speed* c_4 . Especially in the late stages of the giant branch ascension, these assumptions become questionable. Of particular importance is the presence of the coronal dividing line in the HR diagram (Haisch et al. 1991, 1992) to the right of which stars show little x-ray emission and cool winds. Recently, however, ROSAT observations have suggested that many stars do not cross the dividing line in the course of their evolution (Hünsch & Schröder 1996). In particular, stars with $M \gtrsim 1.2M_\odot$ appear to always exhibit coronal activity during the giant phase according to these authors. In that case, our choice of coronal temperature should be reasonable throughout their evolution. However, for less massive single stars, the x-ray emission may drop significantly in the course of their evolution up the giant branch. During the later giant phases of these stars our calculations can only show the qualitative effect of the winds rather than describing them in quantitative detail.

We do allow for the changing stellar radius R_* and stress the rotational and magnetic characteristics of the stellar wind. The use of a one-dimensional Weber-Davis prescription must also be compared to more realistic multi-dimensional stellar wind models quantifying the effect of the changing magnetic topology, as closed field line regions form dead zones from which no mass or AM is lost (cfr. Keppens & Goedbloed 1999; 2000). Nevertheless, we believe that the model gives a fair quantitative indication of the evolving wind influence in the binary systems we studied. As an example, we plot in Fig. 11 the time evolution of the AM loss terms $J_{\text{env}}^{(i)}/\tau_W^{(i)}$ for the system of $1.5M_\odot - 1.25M_\odot$ stars presented in Sect. 3.3. During most of the evolution, the lighter component is responsible for the AM loss. This can be understood from Fig. 12 where the $[f_3, f_5]$ values are

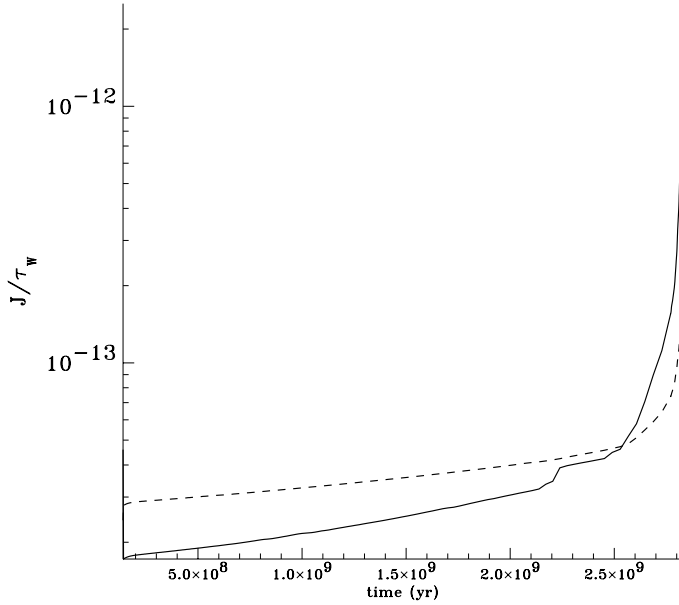


Fig. 11. For Case III: the two AM loss terms associated with the wind of each star (J in 10^{55} cgs units, τ_w in years). The solid line is for the primary $1.5 M_\odot$, the dashed line is for the $1.25 M_\odot$ secondary.

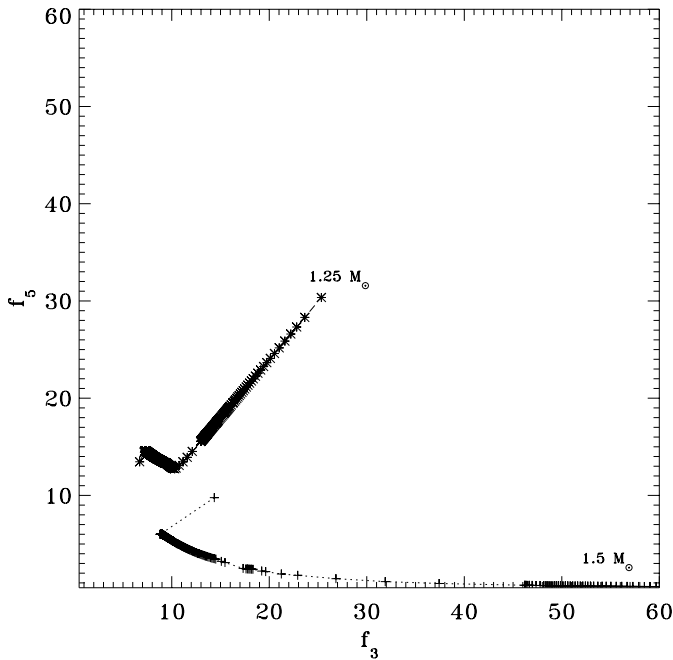


Fig. 12. Case III: the changing character of the wind of each component, as plotted in the $[f_3, f_5]$ landscape. As time progresses, the evolution is towards the labeled endpoint. The first ‘kink’ in the $1.5 M_\odot$ track is due to the immediate synchronization.

plotted as they change during the evolution. While the heavier component develops a strong centrifugally driven wind (f_3), the lighter star has a significant magneto-centrifugal driving effect in its wind (f_5). As a result, the system AM can be shed most effectively by the wind of the secondary.

References

- Alexander D.R., Fergusson J.W., 1994, *ApJ* 437, 879
 Applegate J.H., 1992, *ApJ* 385, 621
 Belcher J.W., MacGregor K.B., 1976, *ApJ* 210, 498
 Bouvier J., Forestini M., Allain S., 1997, *A&A* 326, 1023
 Cassinelli J.P., Lamers H.J.G.L.M., 1987, In: Y. Kondo et al. (eds.), *Exploring the universe in the ultraviolet with the IUE satellite*. Dordrecht: Reidel, p. 139
 Caughlan G.R., Fowler W.A., 1988, *Atomic Data Nuc. Data Tables* 40,2 83
 Charbonneau P., MacGregor K.B., 1992a, *ApJ* 387, 639
 Charbonneau P., MacGregor K.B., 1992b, *ApJ* 397, L63
 Claret A., Giménez A., Cunha N.C.S., 1995, *A&A* 299, 724
 Claret A., Cunha N.C.S., 1997, *A&A* 318, 187
 Dupree A.K., Reimers D., 1987, In: Kondo Y. et al. (eds.), *Exploring the universe in the ultraviolet with the IUE satellite*. Dordrecht: Reidel, p. 321
 Eggleton P.P., Kiseleva L.G., Hut P., 1998, *ApJ* 499, 853
 Goodman J., Dickson E.S., 1998, *ApJ* 507, 938
 Grevesse N., Noels A., 1993, In: Prantzos N., Vangioni-Flam E., Cassé M. (eds.), *Origin and Evolution of the Elements*. Cambridge University Press
 Habets G.M.H.J., Zwaan C., 1989, *A&A* 211, 56
 Haisch B., Schmitt J.H.M.M., Rosso C., 1991, *ApJ* 383, L15
 Haisch B., Schmitt J.H.M.M., Fabian A.C., 1992, *Nat* 360, 239
 Hall D.S., 1991, *ApJ* 380, L85
 Hall D.S., Kreiner J.M., Shore S.N., 1980, In: Plavec M.J., Popper D.M., Ulrich R.K. (eds.), *Close Binary Stars: Observations and Interpretation*, IAU Symp. 88, 383
 Hünsch M., Schröder K.-P., 1996, *A&A* 309, L51
 Iglesias C.A., Rogers F.J., 1996, *ApJ* 464, 943
 Keppens R., 1997, *A&A* 318, 275 (Paper I)
 Keppens R., Goedbloed J.P., 1999, *A&A* 343, 251
 Keppens R., Goedbloed J.P., 2000, *ApJ* 530, 1036
 Keppens R., Charbonneau P., MacGregor K.B., Brandenburg A., 1994, In: Caillault J.-P. (ed.), *Cool Stars, Stellar Systems, and the Sun*, Eighth Cambridge Workshop, ASP Conference Series 64, p. 193
 Keppens R., MacGregor K.B., Charbonneau P., 1995, *A&A* 294, 469
 Lanza A.F., Rodonò M., Rosner R., 1998, *MNRAS* 296, 893
 Maceroni C., 1993, In: Weiss W.W., Baglin A. (eds.), *Inside the Stars*, IAU Colloquium 137, ASP Conference Series 40, p. 374
 MacGregor K.B., Brenner M., 1991, *ApJ* 376, 204
 Moss D., 1986, *MNRAS* 218, 247
 Popper D.M., 1988, *AJ* 95, 1242
 Popper D.M., 1990, *AJ* 100, 247
 Schrijver C.J., Zwaan C., 1991, *A&A* 251, 183
 Skumanich A., 1972, *ApJ* 200, 747
 Solanki S.K., Motamen S., Keppens R., 1997, *A&A* 324, 943
 Stępień K., 1995, *MNRAS* 274, 1019
 Strassmeier K.G., Hall D.S., Fekel F.C., Scheck M., 1993, *A&AS* 100, 173
 Tassoul J.L., Tassoul M., 1992, *ApJ* 395, 259
 Tassoul J.L., Tassoul M., 1996, In: *Fundamentals of Cosmic Physics*, Vol. 16, p. 377
 van ’t Veer F., 1993, In: Leung J.C., Nha I.-S. (eds.), *New Frontiers in binary star research*, ASP Conference Series 38, p. 229
 van ’t Veer F., Maceroni C., 1988, *A&A* 199, 183
 van ’t Veer F., Maceroni C., 1992, In: Duquennoy A., Mayor M. (eds.), *Binaries as tracers of stellar formation*. Cambridge University Press, p. 237
 Weber E.J., Davis L., 1967, *ApJ* 148, 217
 Zahn J.-P., 1977, *A&A* 57, 383
 Zahn J.-P., 1989, *A&A* 220, 112
 Zahn J.-P., Bouchet L., 1989, *A&A* 223, 112